Proceedings of Global Power and Propulsion Society
ISSN-Nr: 2504-4400
GPPS Xi'an21
18th – 20th October, 2021
www.gpps.global

GPPS-TC-2021-0364

Effect of Blade Loading Distribution on Flow Stability of Axial Compressor

Dengke Xu
Beihang University
xudk@buaa.edu.cn
Beijing, China

Xu Dong
Beihang University
buaadongxu@buaa.edu.cn
Beijing, China

Dakun Sun*
Beihang University
sundk@buaa.edu.cn
Beijing, China

Xiaofeng Sun
Beihang University
sunxf@buaa.edu.cn
Beijing, China

ABSTRACT

An efficient and reliable stall inception prediction model is established and integrated into the compressor design. And the effect of blade loading distribution on flow stability of axial compressor is studied via the proposed method. Fore-loaded, aft-loaded and uniformly loaded rotor blades of a subsonic axial compressor are designed by modifying the circulation distribution at the blade region during through-flow calculation. The design criterion is to keep the compressor characteristics unchanged at the design point. The steady numerical simulations of these cases show that the static pressure rise coefficient and adiabatic efficiency of the compressor with aft-loaded rotor blades are the best at small mass flow points, while those for fore-loaded rotor blades are the worst. The flow stability analysis of these cases via the developed model indicates that the compressor with aft-loaded rotor blades has the best stall margin, while that of the compressor with fore-loaded rotor blades is the worst. The steady flow fields are analyzed to reveal the effect mechanism, and the analysis confirms the above conclusion.

INTRODUCTION

As a pivotal design parameter, blade loading is an important indicator of the pressure rise capacity of compressors. Increasing the blade loading to make compressors more compact is an eternal pursuit for modern aero-engines.

Considerable previous studies reveal that the loading distribution on the blade surface directly determines the flow structure in the compressor including the primary flow and the secondary flow, and therefore has a quite significant impact on compressor characteristics incorporating the stall-free operating range. Experiments in a low speed four stage compressor carried out by Wisler (Wisler, 1985) show that the tip aft-loaded rotor has higher efficiency at both design and other operating points than the prototype rotor. In addition, the tip aft-loaded rotor has lower surface peak velocity on the suction side, reduced negative incidence angle and smaller deviation angle. In order to study the effect of blade loading on centrifugal compressor performance, Shibata et al. (Shibata et al., 2012) designed four kinds of fully shrouded impellers by optimizing the blade loading distribution. It was concluded that aft-loading coupled with a high degree of reaction is a really effective way to improve the stall margin as well as stage efficiency. In 2007, Pampreen (Pampreen, 2007) implemented a cascade blade loading analysis by deriving an equation that relates loading to the geometry of the blade and the local change of angular momentum. The blade loading equation is under the assumption of isentropic flow with irrotational motion in the free stream flow field between blades. In accordance with the form of this equation, the blade number, blade wrap angle, blade length and the magnitude of the mean velocity between blades are identified as the principal factors that influence the blade loading. The blade loading calculation for cascades indicates that low loss and maximum stall-free range are associated with zero or slightly negative leading edge loading and about uniform loading between the leading and trailing edges. In 2013, the variation of compressor efficiency with rotor tip clearance is numerically simulated by Sakulkaew et al. (Sakulkaew et al., 2013). The results reveal three different behaviours of

efficiency changing with tip clearance. For relatively large tip clearance, as the blade tip becomes more aft-loaded, the sensitivity of efficiency to tip clearance decreases. Therefore, they believe that in order to eliminate the sensitivity of compressor performance with tip clearance, the rotor should be tip aft-loaded and hub fore-loaded, while the stator should be tip fore-loaded and hub aft-loaded as much as possible. Subsequently, Tiralap et al. (Tiralap et al., 2017) supplemented the optimum loading distribution mode of rotor and stator blades proposed by Sakulkaew et al. (Sakulkaew et al., 2013), and explained the physical flow mechanism behind the influence of the fore- and aft-loaded tip on the compressor characteristics from the point of view of minimizing the loss caused by the tip leakage flow. In conclusion, these existed studies provide us with a valuable perspective to understand the effect of blade loading on flow structure and performance of compressors. However, the blade loading distribution design criteria of these research are not uniform. Therefore, it is necessary to study the influence of loading distribution variation on the compressor performance especially the flow stability on the basis of ensuring the constant total loading on blades from compressor design standpoint. This is of great significance for providing a guidance for designers to choose the parameters of blade loading distribution in the compressor design stage.

At present, it's up to some empirical relationships to ensure the stall margin during the design phase such as the diffusion factor (Lieblein et al., 1953), dimensionless diffusion length (Koch, 1981), solidity of blades and aspect ratio (Wennerstrom, 1989). These empirical methods have a lot of uncertainty and depend on the designer's experience excessively, since they are summarized by a large number of experimental data of cascades and compressors. Therefore, it is necessary to develop a fast and reliable flow stability evaluation tool and combine it with compressor design. From this standpoint, the stall inception prediction model is established based on the general theory of flow instability in turbomachinery (Sun et al., 2013). Differing from the existed analytical model (Stenning, 1980; Moore et al., 1986; Bonnaure, 1991; Sun, 1996) and unsteady numerical simulation (He, 1997), this method not only has the ability to take abundant flow details and the specific blade geometry into consideration, but also has a high computational efficiency. Specifically, based on linear global stability analysis (Theofilis, 2011) and immersed boundary theory (Sirovich, 1967), the non-uniform base flow is regarded as the analysis object, and the blade geometry is described by body force source terms. Eventually, the flow stability problem is transformed into the solution of the eigenvalue equation, and the eigenvalue is the criterion of compressor flow stability.

In the present paper, the stall inception prediction model is developed and integrated into the compressor design. Based on this, the effect of rotor axial blade loading distribution on compressor flow stability is studied and analyzed so as to reveal the effect mechanism from the compressor design viewpoint.

DESIGN OF BLADE LOADING DISTRIBUTION

Based on the frame of turbomachinery design proposed by Wu (Wu, 1951; Wu, 1952), through-flow calculation coupled with three-dimensional blade generation is employed to design the compressor. Streamline curvature method (Novak, 1967) is widely used in engineering because of its clear physical concept, simple formula and fast calculation. Therefore, it is applied for through-flow calculation in the present work. In addition, the mean stream surface method (Gui, 1993) is employed to establish the governing equation of through-flow calculation. Because there are some calculation stations set in the blade region, the solved flow field contains the abundant information of the flow angle of the flow through the blade passage, which is required for blade design. The ultimate blade profile of rotor and stator is generated by employing the blading design method that uses arbitrary camber lines (Gui, 1993). Based on the above compressor design method, a single-stage subsonic axial-flow compressor is used as the object to research different rotor loading distributions. The aerodynamic parameters of the compressor at design operating point are shown in Table 1. And the geometrical parameters are presented in Table 2.

Table 1 Aerodynamic parameters at design operating point

Aerodynamic parameter	
Design speed (rpm)	2930
Mass flow (kg/s)	7.5
Total pressure ratio	1.023
Efficiency	89%

Table 2 Geometrical parameters of the designed compressor

Geometrical parameter	**Rotor**	**Stator**
Number of blades	20	27
Aspect ratio	1.18	1.40
Tip clearance (mm)	0.6	0.5
Shroud diameter (mm)	600	600
Hub diameter (mm)	346	401
Solidity at blade tip	1.4540	1.0963

Solidity at middle blade height	1.5082	1.2418
Solidity at blade root	1.8661	1.5289

The blade loading design is achieved in the through-flow computation. Above all, the circulation CuR in the turbomachinery design is defined as

$$CuR = v \cdot r \,, \tag{1}$$

where v is the circumferential velocity of flow in a stationary reference frame. Then the rotor elementary work l_u at each spanwise position can be expressed as

$$l_u = \frac{2\pi \cdot \Omega}{60} \cdot \left(CuR_2 - CuR_1 \right), \tag{2}$$

where CuR_1 and CuR_2 respectively represent the circulation of each rotor element at the leading edge and trailing edge. And Ω is the rotating speed of rotor, whose unit is r/min. Equation (2) demonstrates that the rotor elementary work depends on the circulation difference of the flow at the trailing edge and leading edge. Therefore, the difference between the flow circulation of a certain axial position in the rotor blade passage and that of the leading edge can reflect the loading of the rotor from the leading edge to this position.

For the single-stage axial-flow compressor in this work, the inlet is in front of the rotor, so the circulation at the leading edge of the rotor is almost zero under the clean inlet flow condition. As a consequence, when redesigning the axial loading distribution of the rotor, the flow circulation at trailing edge of the rotor blade should be kept constant so as to ensure that the rotor work is not been changed at the design operating point.

Because there are several computation stations set inside the blade region, and the flow circulation is the input parameter on each station in through-flow calculation, the rotor blades with different loading distributions can be obtained by designing the circulation distribution of each computation station inside the blade region. In consideration of the comparability of the compressors with different axial loading modes, the radial distribution of the flow circulation on each calculation station remains unchanged. In addition, the flow circulation on the station of non-rotor region including the stator is kept constant. Consequently, the compressors with fore-loaded, uniformly loaded and aft-loaded rotor blades are respectively designed by modifying the axial distribution of the flow circulation on each calculation station inside the rotor region except the leading edge and trailing edge.

STALL INCEPTION PREDICTION METHOD

Stall inception prediction model is established and integrated into the compressor design as a flow stability assessment tool in the present work. The establishing process of the model is briefly introduced in the following part. More details are presented in Ref (He et al., 2018).

In accordance with the immersed boundary theory, the blade geometry in the compressor can be characterized as the source term. Therefore, the flow in the compressor can be governed by the Navier-Stokes (NS) equation with blade force terms. For convenience, the heat conduction and heat generation are neglected in the energy equation. Even though the viscous stress is ignored and not explicitly included in the governing equation, the loss caused by the viscosity in the blade region is considered in the blade force source term. Furthermore, the base flow used for stability analysis is solved via steady viscous simulation, which contains the effect of viscosity. Finally, the governing equation in a stationary reference frame can be written as

$$\begin{cases} \dfrac{\partial \rho}{\partial t} + \nabla \cdot \left(\rho \boldsymbol{u} \right) = 0 \\ \dfrac{\partial \boldsymbol{u}}{\partial t} + \left(\boldsymbol{u} \cdot \nabla \right) \boldsymbol{u} = -\dfrac{1}{\rho} \nabla p + \boldsymbol{f} \\ \dfrac{\partial \left(e + \boldsymbol{u} \cdot \boldsymbol{u} / 2 \right)}{\partial t} + \boldsymbol{u} \cdot \nabla \left(e + \boldsymbol{u} \cdot \boldsymbol{u} / 2 \right) = -\dfrac{1}{\rho} \nabla \cdot \left(p \boldsymbol{u} \right) + \boldsymbol{f} \cdot \boldsymbol{u} \end{cases} \tag{3}$$

where $\boldsymbol{f}$ represents the blade force vector per unit mass, and $\boldsymbol{u}$ is the absolute velocity of flow in the stationary coordinate frame. The pressure, density and internal energy are respectively denoted as p, ρ and e.

Based on the small perturbation theory, the transient flow parameter q can be expressed as the linear superposition of the steady base flow $\bar{q}$ and the unsteady disturbance q',

$$q(r,\theta,z,t) = \bar{q}(r,\theta,z,t) + q'(r,\theta,z,t) \,, \tag{4}$$

where q represents an arbitrary transient flow parameter such as ρ, $\boldsymbol{u}$, p and $\boldsymbol{f}$. r, θ and z are separately radial, circumferential and axial coordinates in the cylindrical coordinate frame. In order to depict the effect of blades on the flow field in compressors, the blade force term is expressed as a strong function of local aerodynamic parameters, that is, $\boldsymbol{f} = f(\rho, \boldsymbol{u}, p)$. According to the first-order Taylor expansion of the blade force with respect to the steady base flow, the perturbation of blade force can be described by

$$\boldsymbol{f}' = \frac{\partial \bar{\boldsymbol{f}}}{\partial \bar{\rho}}\rho' + \frac{\partial \bar{\boldsymbol{f}}}{\partial \bar{u}}u' + \frac{\partial \bar{\boldsymbol{f}}}{\partial \bar{v}}v' + \frac{\partial \bar{\boldsymbol{f}}}{\partial \bar{w}}w' + \frac{\partial \bar{\boldsymbol{f}}}{\partial \bar{p}}p', \tag{5}$$

where u, v and w respectively denote the radial, circumferential and axial velocity in the stationary reference frame.

Due to the unacceptability of memory and computational consumption of three-dimensional eigenvalue matrix, the dimension reduction of the flow is implemented under the assumption of axisymmetric flow. The base flow in this model is in fact the circumferential density-weighted average of the three-dimensional steady flow, and the circumferential partial derivative of the steady physical parameter is zero. By substituting Eq. (4) and Eq. (5) into Eq. (3), subtracting the zero-order equation satisfied by the steady base flow and ignoring the high-order infinitesimal terms, the linearized governing equation with regard to the disturbance can be obtained.

Since the base flow is assumed to be uniform in the circumferential direction, the circumferential modes of small perturbations can be treated as decoupled. Thereby the small perturbation can be expanded by circumferential Fourier expansion and transformed from time domain to frequency domain,

$$q'(r,\theta,z,t)=\hat{q}(r,z)e^{-i\omega t+im\theta}, \tag{6}$$

where $\hat{q}$ represents the amplitude of disturbances, m is the circumferential wave number of perturbations, and ω denotes the system eigenvalue frequency which is a complex.

By substituting and arranging Eq. (6) into the linearized governing equation, the final matrix form of the equation can be described as follows,

$$\left(-i\omega\boldsymbol{A}+\boldsymbol{B}\frac{\partial}{\partial r}+\frac{im}{r}\boldsymbol{C}+\boldsymbol{E}\frac{\partial}{\partial z}+\boldsymbol{G}+\boldsymbol{F}\right)\hat{\boldsymbol{\Phi}}=\boldsymbol{0}, \tag{7}$$

where $\hat{\boldsymbol{\Phi}}=\left(\hat{\rho},\hat{\boldsymbol{u}},\hat{p}\right)^T$ is the column vector composed of the disturbance magnitude. $\boldsymbol{A}$, $\boldsymbol{B}$, $\boldsymbol{C}$, $\boldsymbol{E}$, $\boldsymbol{G}$ and $\boldsymbol{F}$ are coefficient matrices only related to the steady base flow. Among them, the elements in the matrix $\boldsymbol{F}$ are composed of terms related to the blade force, whose details are presented in Ref (He et al., 2018).

According to mathematical theory, the nontrivial solution of the variable $\hat{\boldsymbol{\Phi}}$ in Eq. (7) exists if and only if the determinant of the coefficient matrix is equal to zero, that is,

$$\left|-i\omega\boldsymbol{A}+\boldsymbol{B}\frac{\partial}{\partial r}+\frac{im}{r}\boldsymbol{C}+\boldsymbol{E}\frac{\partial}{\partial z}+\boldsymbol{G}+\boldsymbol{F}\right|=0. \tag{8}$$

It can be seen that the unknown variable in Eq. (8) is only the eigenvalue ω. So far, the eigenvalue equation with respect to the small perturbations is established by supplementing corresponding boundary conditions (He et al., 2018). Then, Eq. (8) is discretized via the spectral collocation method, and the eigenvalue ω is solved by utilizing singular value decomposition (SVD) coupled with traversal algorithm.

The expression of Eq. (6) shows that the real part of the eigenvalue denotes the circumferential propagation speed of the perturbation wave, and the imaginary part reflects the variation of disturbance amplitude with time. If the imaginary part is positive, the perturbations will growth with time until the system instability occurs, and hence the analyzed system is unstable. On the contrary, if the imaginary part is negative, the disturbances will decay over time until they disappears, and therefore the system is stable. Since the circumferential propagation speed of the perturbation wave at the stall inception is the same order of magnitude as the rotating speed of the rotor, the two dimensionless parameters RS (Relative Speed) and DF (Damping Factor) corresponding to the real part and imaginary part of the eigenvalue are defined by using the rotating speed of rotor as a reference value. Their expressions are

$$\begin{aligned} RS &= \frac{\omega_r}{m}\cdot\frac{60}{2\pi\Omega} \\ DF &= \frac{\omega_i}{m}\cdot\frac{60}{2\pi\Omega} \end{aligned}, \tag{9}$$

where ω_r and ω_i are the real part and imaginary part of the eigenvalue ω respectively.

STEADY NUMERICAL SIMULATION

The steady flow fields of the compressors with fore-loaded, uniformly loaded and aft-loaded rotors are separately computed via single-passage steady viscous calculation which simulates the throttling process by gradually increasing the outlet static pressure. After grid independence verification, approximately 1.2 million grids are arranged in the whole computational domain, as shown in Fig. 1. Second order backward Euler scheme and κ-ε turbulence model are employed in the simulation and the rationality is verified by the comparison between the computation and experiments. The total pressure and total temperature at inlet are respectively set to 101325Pa and 288.15K. Mixing plane method is used to deal with the rotor/stator interface. The numerical calculation of the compressor at each mass flow condition is realized by adjusting the static pressure at outlet.

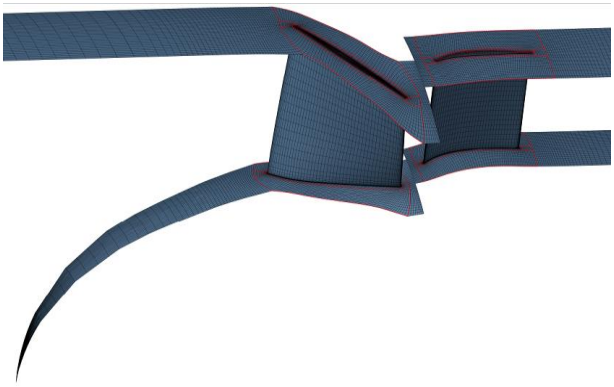

Figure 1 Computational Mesh

Steady Performance

The comparison of overall performance of fore-loaded compressor obtained via steady simulations and experiments is shown in Fig. 2. The static pressure rise coefficient is defined as

$$P_r = \frac{p_o - p_{it}}{\frac{1}{2}\rho_i U_m^2}, \tag{10}$$

where p_o and p_{it} denote the static pressure at outlet and the total pressure at inlet, ρ_i is the density at inlet, U_m represents the tangential velocity of rotor at the middle blade height. It is evident that the calculated static pressure rise coefficients at the whole operating range are in good agreement with the experimental results even though they are slightly higher than experiments at large mass flow points. In general, the last convergence mass flow rate of steady numerical simulation is considered as the steady stall inception point. Compared with the experimental stall limit 5.38kg/s, the relative error of steady stall inception 5.15kg/s is -4.28%.

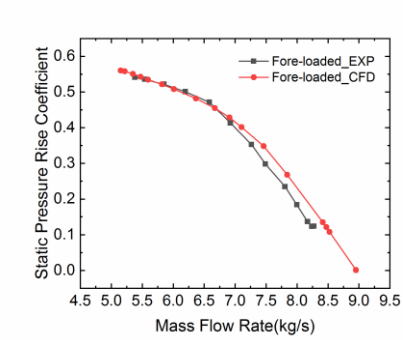

Figure 2 Comparison of the Overall Performance between Steady Simulations and Experiments

The steady performance of the compressors with different axial loading distributions on rotor blades is compared in Fig. 3. It can be seen that the three compressors show the identical characteristics in terms of pressure rise and adiabatic efficiency at the design operating point 7.50kg/s, which is consistent with the original intention of rotor loading design. With regard to the off-design condition, it is obvious that the pressure rise and efficiency of aft-loaded compressor are the best at low mass flow rates, followed by the uniformly loaded compressor, and those of the fore-loaded compressor are the worst. However, the result is opposite for the cases of mass flow larger than the design point. At large mass flow condition, the static pressure rise coefficient and adiabatic efficiency of aft-loaded compressor are slightly smaller than the other two compressors, and the fore-loaded compressor has the best performance.

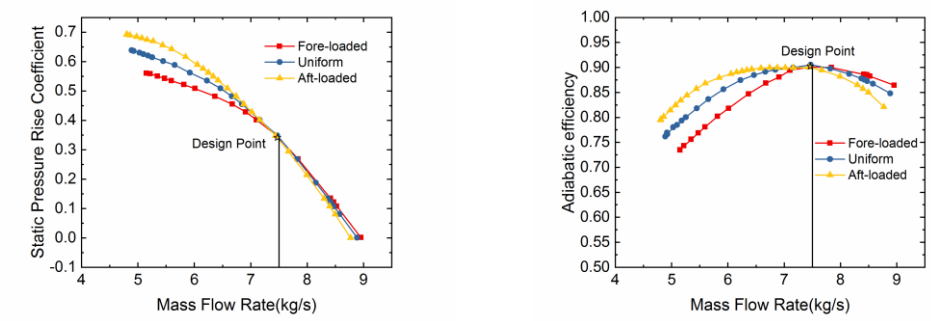

(a) Static Pressure Rise Coefficient **(b) Adiabatic Efficiency**

Figure 3 Comparison of the Three Compressors

Steady Loading of Rotor Blade

In this section, the loading distribution on the rotor blade obtained from the steady simulation will be analyzed to verify whether it meets the design requirements of changing the axial loading mode of the rotor.

The static pressure difference between the suction side and pressure side of the rotor blade is an intuitive parameter that reflects the blade loading. Therefore, the contour of the static pressure difference on the whole rotor blade of the three compressors at design operating point is extracted from the steady flow field and shown in Fig. 4. It is apparent that the axial positions of the peak loading of the fore-loaded, uniformly loaded and aft-loaded rotor blades at the design point are near the leading edge, mid-chord and near the trailing edge respectively, which can also be observed via the circulation distribution at rotor blade region shown in Fig. 5. It is the expected distribution and therefore proves the rationality of axial loading design in through-flow calculation.

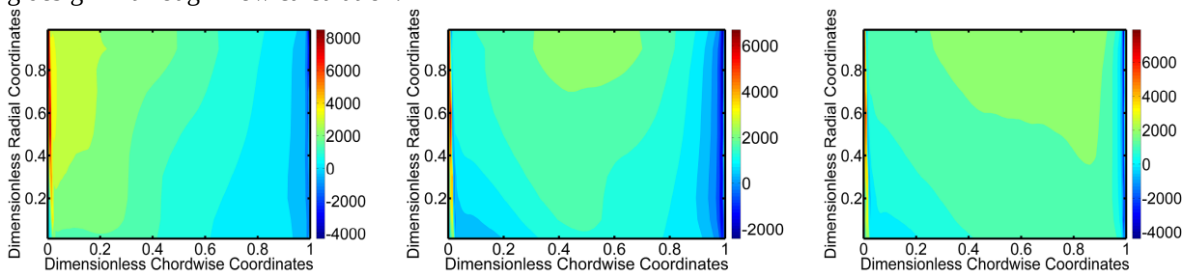

(a) Fore-loaded **(b) Uniformly loaded** **(c) Aft-loaded**

Figure 4 Static Pressure Difference of Rotor Blade at Design Point

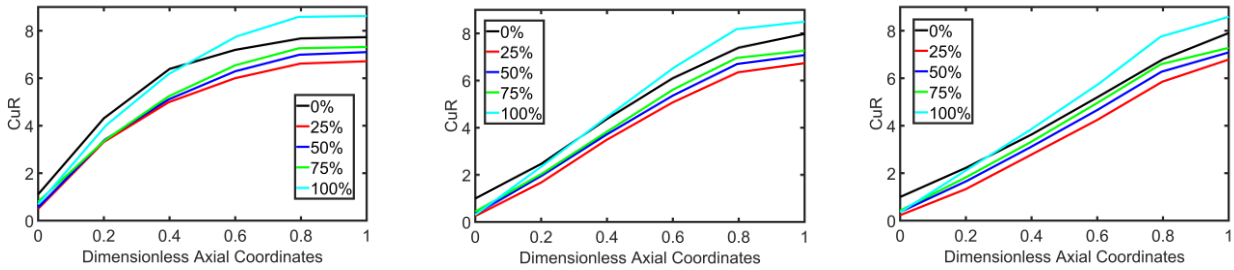

(a) Fore-loaded **(b) Uniformly loaded** **(c) Aft-loaded**

Figure 5 Circulation at Rotor Blade Region at Design Point

In general, the operation condition of the compressor at near-stall point attracts much attention as an important off-design point. Therefore, the steady loading analysis of rotor blades with different axial loading distributions is carried out at the near-stall operating condition. Above all, the static pressure differences between the suction side and pressure side of the rotor blade of the three compressors are analysed and presented in Fig. 6. It is found that compared with the fore-loaded rotor, the uniformly loaded and aft-loaded rotors do move the loading on the rotor blades towards the trailing edge, especially the aft-loaded rotor blades. However, the peak loading positions of the uniformly loaded and aft-loaded rotors are all close to the leading edge at the near-stall operating condition, which is similar to that of the fore-loaded rotor. This is different from that at the design operating point shown in Fig. 4. This finding indicates that when the operating condition of the compressor moves from the design point to near-stall point, the difference of the loading distribution on fore-loaded, uniformly loaded and aft-loaded rotor blades becomes smaller. Moreover, the peak loading positions of the uniformly loaded and aft-loaded rotors move towards the leading edge.

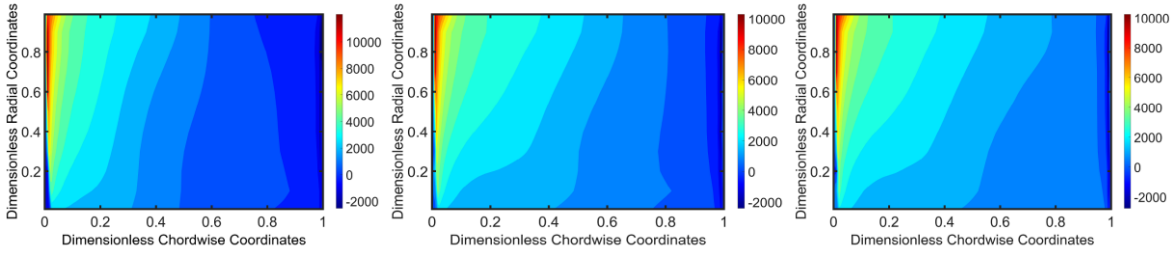

(a) Fore-loaded **(b) Uniformly loaded** **(c) Aft-loaded**

Figure 6 Static Pressure Difference of Rotor Blade at Near-Stall Point

FLOW STABILITY ANALYSIS

First of all, the stall inception point of the compressor with fore-loaded rotor blades is predicted via the developed model so as to verify its accuracy. As mentioned before, the dimensionless parameter DF represents the growth rate of small perturbations, and therefore can be considered as a criterion of whether the current flow system is stable or not. To be specific, the sign mutation of the DF accompanying with the throttling process denotes the occurrence of stall onset.

The flow stability prediction of the three compressors at each operating mass flow condition is presented in Fig. 7. It is found that DF increases accompanying with the throttling process, which characterizes the deterioration process of the compressor flow stability with the operating mass flow rate reducing from the blocking point to the near-stall point. In addition, DF of the fore-loaded compressor is equal to zero at 5.34kg/s. If the mass flow rate continues to decrease, the DF will change from negative to positive, and then the compressor enter instability state. Therefore, the predicted stall inception of the fore-loaded compressor is 5.34kg/s. Compared with the experimental stall point 5.38kg/s, the relative error of the predicted result is only -0.74%, which confirms the prediction precision of the developed flow stability model. Moreover, the stall inception points of uniformly loaded and aft-loaded compressors are 5.16kg/s and 5.06kg/s respectively, which indicates that the flow stability of the aft-loaded compressor is the best among the three compressors, followed by the uniformly loaded compressor, and that of the fore-loaded compressor is the worst.

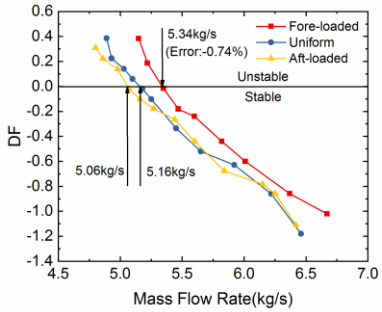

Figure 7 Stall Inception Prediction of the Three Compressors

STEADY FLOW ANALYSIS

In order to reveal the physical mechanism behind the stability variation of the three compressors with different axial loading distributions on rotor blades, the steady flow fields of them are analyzed in depth.

Rotor elementary work at all radial positions of the three compressors at the near-stall operating point is calculated and compared in Fig. 8(a). It can be found that the radial distributions of the rotor elementary work of the three compressors are similar in form. Specifically, the rotor elementary work near the tip is significantly larger than that at other radial positions. This result indicates that the tip part of the rotor blade has the largest loading compared with other radial positions, which can also be observed in Fig. 6. The larger the loading is, the more difficult it is for the blade to organize the flow. Therefore, the flow condition at the tip region is the worst in all radial positions. As shown in Fig. 8(a), the elementary work of aft-loaded compressor is larger than the other two compressors at the radial position below 85% of the blade height, and that of fore-loaded compressor is minimum, which is the main reason for the pressure rise difference among the three compressors at low mass flow conditions presented in Fig. 3(a). However, it is evident that the maximum elementary work at the blade tip of the fore-loaded compressor is the largest among the three compressors at the near-stall operating point, while that of the aft-loaded compressor is the smallest, which means that the blade loading at the rotor tip increases and thus the flow situation gets worse as the rotor becomes more fore-loaded. This analysis explains the flow stability prediction result shown in Fig. 7.

The circulation difference between the trailing edge and leading edge of the stator at the near-stall operating point can be considered as an indicator of the loading level on the stator blade, which is calculated and presented in Fig. 8(b). It can be seen that the stator circulation difference of the three compressors near the tip is the largest in all radial positions, which indicates that the stator blade loading at the tip region is the largest and thus the flow condition is the worst compared with other radial positions. With emphasis on the tip region, it is obvious that the stator circulation difference of the fore-loaded compressor is larger than that of the other two compressors, and that of the aft-loaded compressor is the smallest. Therefore, the flow situation at the tip of stator in the fore-loaded compressor is the worst among the three compressors, followed by the uniformly loaded compressor, and that in the aft-loaded compressor is the best. This trend is consistent with the analysis shown in Fig. 8(a).

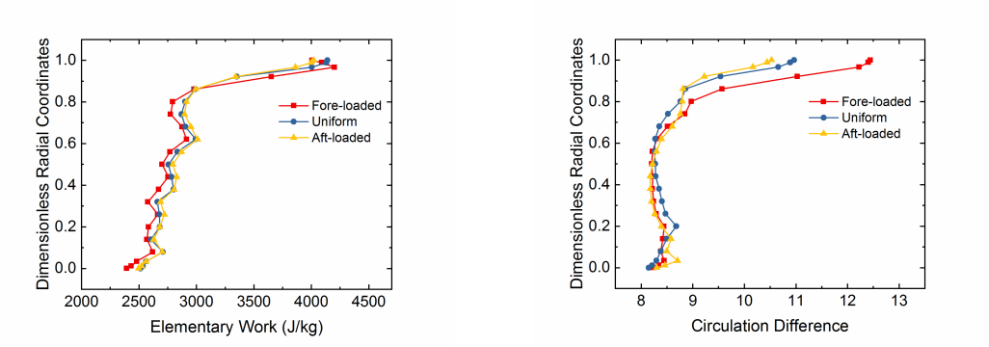

(a) Rotor Elementary Work **(b) Stator Circulation Difference**

Figure 8 Rotor Elementary Work and Stator Circulation Difference at Near-Stall Point

CONCLUSIONS

Three compressors with fore-loaded, uniformly loaded and aft-loaded rotor blades are designed based on the through-flow calculation coupled with the blading design method that uses arbitrary camber lines. Steady numerical simulations indicate that peak loading positions on the rotor blades of the three compressors are consistent with the original intention of the design at the design operating condition, and they move to the leading edge accompanying with the throttling process. Overall performance including pressure rise and adiabatic efficiency of the three compressors is identical at the design operating point. However, at low mass flow conditions, the pressure rise and efficiency of the aft-loaded compressor are the best, followed by the uniformly loaded compressor, and those of fore-loaded compressor are the worst. The opposite is true at large mass flow points.

A stall inception prediction model is established and integrated into the compressor design system. The flow stability prediction results of the three compressors present that the fore-loaded compressor is the first to enter instability state, followed by the uniformly loaded compressor, while the aft-loaded compressor is the last. The steady flow fields reveal that the maximum tip loading of rotor blades becomes larger at the near-stall point as the rotor becomes more fore-loaded, which explains the flow stability distinction of the three compressors to some extent.

NOMENCLATURE

$\boldsymbol{A}, \boldsymbol{B}, \boldsymbol{C}, \boldsymbol{E}, \boldsymbol{G}$	=	coefficient matrixes
CuR	=	flow circulation
DF	=	damping factor
e	=	internal energy
$\boldsymbol{F}$	=	a matrix related to blade force
f	=	blade force vector per unit mass
i	=	imaginary unit
l_u	=	elementary work
m	=	circumferential wave number
P_r	=	static pressure rise coefficient
p	=	static pressure
p_o	=	static pressure at outlet
p_{it}	=	total pressure at inlet
q	=	an arbitrary transient flow parameter
RS	=	relative speed
r, θ, z	=	cylindrical coordinates
t	=	time
$\boldsymbol{u}$	=	absolute velocity vector
u	=	radial velocity
v	=	circumferential velocity
w	=	axial velocity
ρ	=	density
ρ_i	=	density at inlet

$\boldsymbol{\Phi}$	=	column vector of perturbations
Ω	=	rotating speed of rotors
ω	=	complex eigenvalue
∇	=	gradient operator
$\nabla\cdot$	=	divergence operator
Subscripts		
i	=	imaginary part
r	=	real part
1	=	at the leading edge
2	=	at the trailing edge
Superscripts		
T	=	transposition
$\hat{}$	=	amplitude of perturbation
'	=	perturbation quantity
—	=	base quantity

ACKNOWLEDGMENTS

The research presented here is supported by National Natural Science Foundation of China (Nos. 51822601, 51790514 and 51906004) and National Science and Technology Major Project (2017-II-0005-0018). Also, the research is supported by the Academic Excellence Foundation of BUAA for PhD Students.

REFERENCES

Bonnaure, L. P. (1991). *Modelling High Speed Multistage Compressor Stability*. M.S. Cambridge.

Gui, X. (1993). *Research on the Model of Controllable Shock Wave in the Design of Transonic Axial Fan/Compressor Stages*. Ph.D. Beihang University.

He, C., Ma, Y., Liu, X., Sun, D., and Sun, X. (2018). Aerodynamic Instabilities of Swept Airfoil Design in Transonic Axial-Flow Compressors. *AIAA Journal*, 56(5), pp. 1-16.

He, L. (1997). Computational Study of Rotating-Stall Inception in Axial Compressors. *AIAA Journal of Propulsion and Power*, 13(1), pp. 31-38.

Koch, C. C. (1981). Stalling Pressure Rise Capability of Axial Flow Compressor Stages. *ASME Journal of Engineering for Gas Turbines and Power*, 103(4), pp. 645-656.

Lieblein, S., Schwenk, F. C., and Broderick, R. L. (1953). Diffusion Factor for Estimating Losses and Limiting Blade Loadings in Axial-Flow-Compressor Blade Elements. NACA RM E53D01.

Moore, F. K., and Greitzer, E. M. (1986). A Theory of Post-Stall Transients in Axial Compression Systems: Part I-Development of Equations. *ASME Journal of Engineering for Gas Turbines and Power*, 108(1), pp. 68-76.

Novak, R. A. (1967). Streamline Curvature Computing Procedures for Fluid-Flow Problems. *ASME Journal of Engineering for Power*, 89(4), pp. 478-490.

Pampreen, RC. (2007). Cascade Blade Loading Analysis With Application to Turbomachinery Design. *Proceedings of the ASME 2007 International Mechanical Engineering Congress and Exposition*, Washington, USA, No. IMECE2007-41398, pp. 771-787.

Sakulkaew, S., Tan, C. S., Donahoo, E., Cornelius, C., and Montgomery, M. (2013). Compressor Efficiency Variation With Rotor Tip Gap From Vanishing to Large Clearance. *ASME Journal of Turbomachinery*, 135(3), pp. 031030.

Shibata, T., Yagi, M., Nishida, H., Kobayashi, H., and Tanaka, M. (2012). Effect of Impeller Blade Loading on Compressor Stage Performance in a High Specific Speed Range. *ASME Journal of Turbomachinery*, 134(4), pp. 041012.

Sirovich, L. (1967). Initial and Boundary Value Problems in Dissipative Gas Dynamics. *Physics of Fluids*, 10(1), pp. 24-34.

Stenning, A. H. (1980). Rotating Stall and Surge. *ASME Journal of Fluids Engineering*, 102(1), pp. 14-20.

Sun, X. (1996). On the Relation Between the Inception of Rotating Stall and Casing Treatment. *Joint Propulsion Conference and Exhibit 1996*, AIAA Paper 1996-2579.

Sun, X., Liu, X., Hou, R., and Sun, D. (2013). A General Theory of Flow-Instability Inception in Turbomachinery. *AIAA Journal*, 51(7), pp. 1675-1687.

Theofilis, V. (2011). Global Linear Instability. *Annual Review of Fluid Mechanics*, 43(1), pp. 319-352.

Tiralap, A., Tan, C. S., Donahoo, E., Montgomery, M., and Cornelius, C. (2017). Effects of Rotor Tip Blade Loading Variation on Compressor Stage Performance. *ASME Journal of Turbomachinery*, 139(5), pp. 051006.

Wennerstrom, A. J. (1989). Low Aspect Ratio Axial Flow Compressors: Why and What It Means. *ASME Journal of Turbomachinery*, 111(4), pp. 357-365.
Wisler, D. C. (1985). Loss Reduction in Axial-Flow Compressors Through Low-Speed Model Testing. *ASME Journal of Engineering for Gas Turbines and Power*, 107(2), pp. 354-363.
Wu, C. H. (1951). A General Through-Flow Theory of Fluid Flow with Subsonic or Supersonic Velocity in Turbomachines of Arbitrary Hub and Casing Shapes. NACA TN 2302.
Wu, C. H. (1952). A General Theory of Three-Dimensional Flow in Subsonic and Supersonic Turbomachines of Axial-, Radial-, and Mixed-Flow Types, NACA TN 2604.